



## Combined Upper Limits on Standard Model Higgs Boson Production from the DØ Experiment in 1.0-2.3 fb<sup>-1</sup>

The DØ Collaboration  
URL <http://www-d0.fnal.gov>  
(Dated: March 10, 2008)

Searches for standard model Higgs boson production in  $p\bar{p}$  collisions at  $\sqrt{s} = 1.96$  TeV have been carried out for Higgs boson masses ( $m_H$ ) in the range  $105 < m_H < 200$  GeV/ $c^2$ . The contributing production processes include associated production ( $WH \rightarrow \ell\nu b\bar{b}$ ,  $ZH \rightarrow \ell\ell/\nu\nu b\bar{b}$ ,  $WH \rightarrow WW^+W^-$ ), gluon fusion ( $H \rightarrow W^+W^-$ ,  $H \rightarrow \gamma\gamma$ ), and vector boson fusion ( $qq'H \rightarrow qq'W^+W^-$ ). Analyses are conducted with integrated luminosities from 1.0 fb<sup>-1</sup> to 2.3 fb<sup>-1</sup>. As no significant excess is observed, we proceed to set limits on standard model Higgs boson production. The observed 95% confidence level upper limits are found to be a factor of 6.4 (2.2) higher than the predicted standard model cross section at  $m_H = 115$  (160) GeV/ $c^2$  while the expected limits are found to be a factor of 5.5 (2.4) higher than the standard model cross section for the same masses.

## I. INTRODUCTION

Despite its success as a predictive tool, the standard model (SM) of particle physics remains incomplete without a means to explain electroweak symmetry breaking. The simplest proposed mechanism involves the introduction of a complex doublet of scalar fields that generate the masses of elementary particles via their mutual interactions. After accounting for longitudinal polarizations for the electroweak bosons, this so-called Higgs mechanism also gives rise to a single scalar boson with an unpredicted mass. Direct searches in  $e^+e^- \rightarrow Z^* \rightarrow ZH$  at the Large Electron Positron (LEP) collider yielded lower mass limits at  $m_H > 114.4 \text{ GeV}/c^2$  [1] while precision electroweak data yield the indirect constraint  $m_H < 144 \text{ GeV}/c^2$  [2], with both limits set at 95% confidence level (C.L.). When also considering the direct limit, the indirect constraint predicts  $m_H < 182 \text{ GeV}/c^2$ , indicating that the range  $110 \leq m_H \leq 200 \text{ GeV}/c^2$  is the most important search region for a SM Higgs boson. The search for a SM Higgs boson is one of the main goals of the Fermilab Tevatron physics program.

In this note, we combine recent results for direct searches for SM Higgs bosons in  $p\bar{p}$  collisions at  $\sqrt{s} = 1.96 \text{ TeV}$  recorded by the DØ experiment [3]. These are searches for Higgs bosons produced in association with vector bosons ( $p\bar{p} \rightarrow WH \rightarrow \ell\nu b\bar{b}$ ,  $p\bar{p} \rightarrow ZH \rightarrow \ell\ell/\nu\nu b\bar{b}$  and  $p\bar{p} \rightarrow WH \rightarrow WW^+W^-$ ), quarks ( $p\bar{p} \rightarrow q\bar{q}H \rightarrow q\bar{q}W^+W^-$ ) or through gluon-gluon fusion ( $p\bar{p} \rightarrow H \rightarrow W^+W^-$ ,  $p\bar{p} \rightarrow H \rightarrow \gamma\gamma$ ). The searches were conducted with data collected during the period 2002-2007 and correspond to integrated luminosities ranging from  $1.0 \text{ fb}^{-1}$  to  $2.3 \text{ fb}^{-1}$ . The searches are organized into fifteen final states, each designed to isolate a particular Higgs boson production and decay mode. In order to facilitate proper combination of signals, the analyses were designed to be mutually exclusive after analysis selections. Searches for several final states are performed in two distinct epochs of data collection: before and after the 2006 DØ detector upgrade. The largest changes made during the upgrade were the addition of a new layer to the silicon detector nearest to the beam-line and an upgrade of the trigger system. The two epochs are denoted as Run IIa ( $1.1 \text{ fb}^{-1}$ ) and Run IIb ( $1.2 \text{ fb}^{-1}$ ). This results in a total of 25 individual analyses.

The 25 analyses [4–10] are outlined in Table I. In the cases of  $p\bar{p} \rightarrow W/ZH + X$  production, we search for a Higgs boson decaying to two bottom-quarks. The decays of the vector bosons further define the analyzed final states:  $WH \rightarrow \ell\nu b\bar{b}$ ,  $ZH \rightarrow \ell\ell b\bar{b}$  and  $ZH \rightarrow \nu\bar{\nu} b\bar{b}$ . In order to isolate  $H \rightarrow b\bar{b}$  decays, an algorithm for identifying jets consistent with the decay of a heavy-flavor quark is applied to each jet (*i.e.*  $b$ -tagging). Several kinematic variables sensitive to transversely-displaced jet vertices and jet tracks with large transverse impact parameters relative to the hard-scatter vertices are combined in a neural network (NN) discriminant trained to identify real heavy-flavor quark decays and reject jets arising from light-flavor quarks or gluons [11]. By adjusting a minimum requirement on the  $b$ -tagging NN output, a spectrum of increasingly stringent  $b$ -tagging operating points is achieved, each with a different signal efficiency and purity. For the  $WH \rightarrow \ell\nu b\bar{b}$  and  $ZH \rightarrow \ell\ell b\bar{b}$  processes, the analyses are separated into two groups: one in which two of the jets were  $b$ -tagged with a loose tagging requirement (herein called double  $b$ -tag or DT) and one group in which only one jet was tagged with a tight tag algorithm (single  $b$ -tag or ST). The ST selection excludes additional loose-tagged jets, rendering the ST and DT selections orthogonal. The ST selection results in a typical per-jet efficiency and fake rate of about 60% and 1.5%, while the DT selection gives 50% and 0.5%, respectively. For these analyses, each lepton flavor of the  $W/Z$  boson decay ( $\ell = e, \mu$ ) is treated as an independent channel. For the  $ZH \rightarrow \nu\bar{\nu} b\bar{b}$  analyses, two or three jets are required in the final state with the two leading jets satisfying a loose  $b$ -tag and one of these jets also satisfying a tight  $b$ -tag. In the case of  $WH \rightarrow \ell\nu b\bar{b}$  production, the primary lepton from the  $W$  boson decay may fall outside of the detector fiducial volume or is not identified. This case is treated as a separate  $WH$  analysis, referred to as  $WH \rightarrow \ell\nu b\bar{b}$ . For this channel, the background is the same as for the  $ZH \rightarrow \nu\bar{\nu} b\bar{b}$  analysis.

We also consider Higgs decays to two  $W^\pm$  bosons. For  $WH \rightarrow WW^+W^-$  production, we search for leptonic  $W$  boson decays with three final states of same-signed leptons:  $WWW \rightarrow e^\pm \nu e^\pm \nu + X$ ,  $e^\pm \nu \mu^\pm \nu + X$ , and  $\mu^\pm \nu \mu^\pm \nu + X$ . In the case of  $p\bar{p} \rightarrow H \rightarrow W^+W^-$  and  $p\bar{p} \rightarrow q\bar{q}H \rightarrow q\bar{q}W^+W^-$  production, we search for leptonic  $W$  boson decays with three final states of opposite-signed leptons:  $WW \rightarrow e^+ \nu e^- \nu$ ,  $e^\pm \nu \mu^\mp \nu$ , and  $\mu^+ \nu \mu^- \nu$ . For the gluon fusion and vector boson fusion processes,  $H \rightarrow b\bar{b}$  decays are not considered due to the large multijets background. In all  $H \rightarrow W^+W^-$  decays with  $m_H < 2M_W$ , one of the  $W$  bosons will be off mass shell. In all cases, lepton selections include both electrons and muons ( $\ell = e, \mu$ ), but  $\tau$  leptons are included in the simulation and the selections necessarily have acceptance for secondary leptons from  $\tau \rightarrow \nu e, \mu \nu$  decays. Finally, we include two analyses (Run IIa and Run IIb) that search for Higgs bosons produced via gluon fusion and decaying to two photons.

Since the most recent DØ SM combined Higgs boson search results [12], we have updated the Run IIa  $ZH \rightarrow \nu\bar{\nu} b\bar{b}$  analysis and the Run IIb  $H \rightarrow W^+W^-$  analyses. The Run IIb  $ZH \rightarrow \nu\bar{\nu} b\bar{b}$  analysis and the  $H \rightarrow \gamma\gamma$  analyses are new and are for the first time included into this combination.

Higgs signals are simulated using PYTHIA [13] using CTEQ6L1 and CTEQ6M ( $H \rightarrow W^+W^-$  Run IIb) [14] leading order parton distribution functions. The signal cross sections are normalized to next-to-next-to-leading-order (NNLO) calculations [15, 16] and branching ratios are calculated using HDECAY [17]. The  $H \rightarrow W^+W^-$  signal cross sections calculations also contain next-to-next-to-leading-logarithm corrections. The contributions from QCD

TABLE I: List of analysis channels, corresponding integrated luminosities, and final variables. See Sect. I for details. The final variable used for several analyses is a neural-network or boosted decision-tree discriminant output which is abbreviated as “NN discriminant” and “DTree discriminant”, respectively.

Channel	Data Epoch	Luminosity ( $\text{fb}^{-1}$ )	Final Variable	Reference
$WH \rightarrow \mu\nu b\bar{b}$ , ST/DT	Run IIa	1.05	NN discriminant	[4]
$WH \rightarrow \mu\nu b\bar{b}$ , ST/DT	Run IIb	0.63	NN discriminant	[4]
$WH \rightarrow e\nu b\bar{b}$ , ST/DT	Run IIa	1.04	NN discriminant	[4]
$WH \rightarrow e\nu b\bar{b}$ , ST/DT	Run IIb	0.64	NN discriminant	[4]
$WH \rightarrow \ell\nu b\bar{b}$ , DT	Run IIa	0.90	DTree discriminant	[5]
$WH \rightarrow \ell\nu b\bar{b}$ , DT	Run IIb	1.18	DTree discriminant	[5]
$ZH \rightarrow \nu\bar{\nu} b\bar{b}$ , DT	Run IIa	0.90	DTree discriminant	[5]
$ZH \rightarrow \nu\bar{\nu} b\bar{b}$ , DT	Run IIb	1.18	DTree discriminant	[5]
$ZH \rightarrow \mu^+\mu^- b\bar{b}$ , ST/DT	Run IIa	1.10	NN discriminant	[6]
$ZH \rightarrow e^+e^- b\bar{b}$ , ST/DT	Run IIa	1.10	NN discriminant	[6]
$WH \rightarrow WW^+W^- (\mu^\pm\mu^\pm)$	Run IIa	1.00	2-D Likelihood	[7]
$WH \rightarrow WW^+W^- (e^\pm\mu^\pm)$	Run IIa	1.00	2-D Likelihood	[7]
$WH \rightarrow WW^+W^- (e^\pm e^\pm)$	Run IIa	1.00	2-D Likelihood	[7]
$H \rightarrow W^+W^- (\mu^+\mu^-)$	Run IIa	1.10	NN discriminant	[8]
$H \rightarrow W^+W^- (e^\pm\mu^\mp)$	Run IIa	1.10	NN discriminant	[8]
$H \rightarrow W^+W^- (e^+e^-)$	Run IIa	1.10	NN discriminant	[8]
$H \rightarrow W^+W^- (\mu^+\mu^-)$	Run IIb	1.20	NN discriminant	[9]
$H \rightarrow W^+W^- (e^\pm\mu^\mp)$	Run IIb	1.20	NN discriminant	[9]
$H \rightarrow W^+W^- (e^+e^-)$	Run IIb	1.20	NN discriminant	[9]
$H \rightarrow \gamma\gamma$	Run IIa	1.10	Di-photon Invariant Mass	[10]
$H \rightarrow \gamma\gamma$	Run IIb	1.20	Di-photon Invariant Mass	[10]

multijet production are measured in data. The other backgrounds were generated by PYTHIA, ALPGEN [18], and COMPEP [19], with PYTHIA providing parton-showering and hadronization. Background cross sections are either normalized to next-to-leading order (NLO) calculations from MCFM [20] or to data control samples whenever possible.

## II. LIMIT CALCULATIONS

We combine results using the  $CL_s$  method with a log-likelihood ratio (LLR) test statistic [21]. The value of  $CL_s$  is defined as  $CL_s = CL_{s+b}/CL_b$  where  $CL_{s+b}$  and  $CL_b$  are the confidence levels for the signal-plus-background hypothesis and the background-only hypothesis, respectively. These confidence levels are evaluated by integrating corresponding LLR distributions populated by simulating outcomes via Poisson statistics. Separate channels and bins are combined by summing LLR values over all bins and channels. This method provides a robust means of combining individual channels while maintaining individual channel sensitivities and incorporating systematic uncertainties. Systematics are treated as Gaussian uncertainties on the expected numbers of signal and background events, not the outcomes of the limit calculations. This approach ensures that the uncertainties and their correlations are propagated to the outcome with their proper weights. The  $CL_s$  approach used in this analysis utilizes binned final-variable distributions rather than a single-bin (fully integrated) value for each contributing analysis.

### A. Final Variable Preparation

For the  $WH \rightarrow \ell\nu b\bar{b}$ ,  $ZH \rightarrow \ell\bar{\ell} b\bar{b}$ , and  $H \rightarrow W^+W^-$  analyses, the final variable used for limit setting is the output of a neural-network (NN) discriminant, trained separately for each Higgs boson mass tested. For the Run IIa  $H \rightarrow W^+W^-$  analyses, each NN is constructed using kinematic variables which may be different for each Higgs boson mass. The  $WH \rightarrow WW^+W^-$  analysis utilizes a two-dimensional likelihood discriminant as a final variable and the  $ZH \rightarrow \nu\bar{\nu} b\bar{b}$  analyses employ a boosted decision-tree discriminant. Several background components of the final variables are smoothed via Gaussian kernel estimation [22] to minimize fluctuations in the shape of the final variable arising from the limited statistics of the simulated samples. The final variables for all analyses are shown in Figs. 1-4, including any smoothing processes.

To decrease the granularity of the steps between simulated Higgs boson masses in the limit calculation, additional mass points are created via interpolation [23]. The primary motivation of this procedure is to provide a means of combining analyses which do not share a common simulated Higgs boson mass. However, this procedure also allows a measurement of the behavior of each limit on a finer granularity than otherwise possible. We report results only for mass points which contain a minority of interpolated analyses.

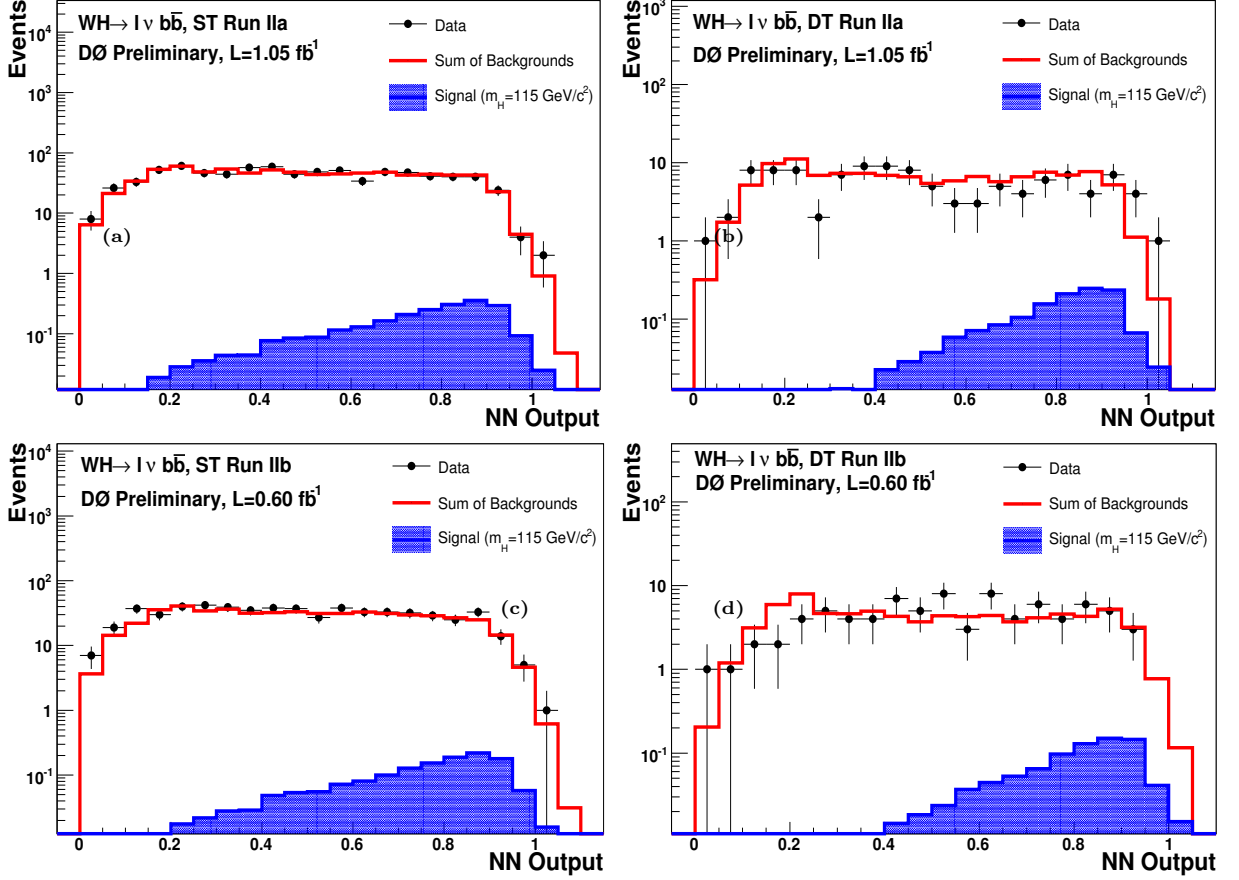


FIG. 1: Final variable distributions for  $p\bar{p} \rightarrow WH \rightarrow \ell\nu b\bar{b}$  Higgs search analyses. The figure contains distributions for: the NN discriminant for the Run IIa  $WH \rightarrow \ell\nu b\bar{b}$  ST analyses (a), the NN discriminant for the Run IIa  $WH \rightarrow \ell\nu b\bar{b}$  DT analyses (b), the NN discriminant for the Run IIb  $WH \rightarrow \ell\nu b\bar{b}$  ST analyses (c), and the NN discriminant for the Run IIb  $WH \rightarrow \ell\nu b\bar{b}$  DT analyses (d). For each figure, the total signal and background expectations and the observed data are shown.

## B. Systematic Uncertainties

The systematic uncertainties differ between analyses for both the signals and backgrounds [4–10]. Here we will summarize only the largest contributions. Most analyses carry an uncertainty on the integrated luminosity of 6.1%, while the overall normalization of other analyses is determined from the NNLO  $Z/\gamma^*$  cross section in data events near the peak of  $Z \rightarrow \ell\ell$  decays in data. The  $H \rightarrow b\bar{b}$  analyses have an uncertainty on the  $b$ -tagging rate of 4-6% per tagged jet. These analyses also have an uncertainty on the jet measurement and acceptances of  $\sim 7.5\%$ . For the  $H \rightarrow W^+W^-$  analyses we include uncertainties associated with lepton measurement and acceptances, which range from 3-6% depending on the final state. The largest contribution for all analyses is the uncertainty on the background cross sections at 6-30% depending on the analysis channel and specific background. These values include both the uncertainty on the theoretical cross section calculations and the uncertainties on the higher order correction factors. The uncertainty on the expected multijet background is dominated by the statistics of the data sample from which it is estimated, and is considered separately from the other cross section uncertainties. The  $p\bar{p} \rightarrow H \rightarrow W^+W^-$  analyses are also assigned a 10% uncertainty on the NNLO Higgs production cross section associated with the accuracy of the

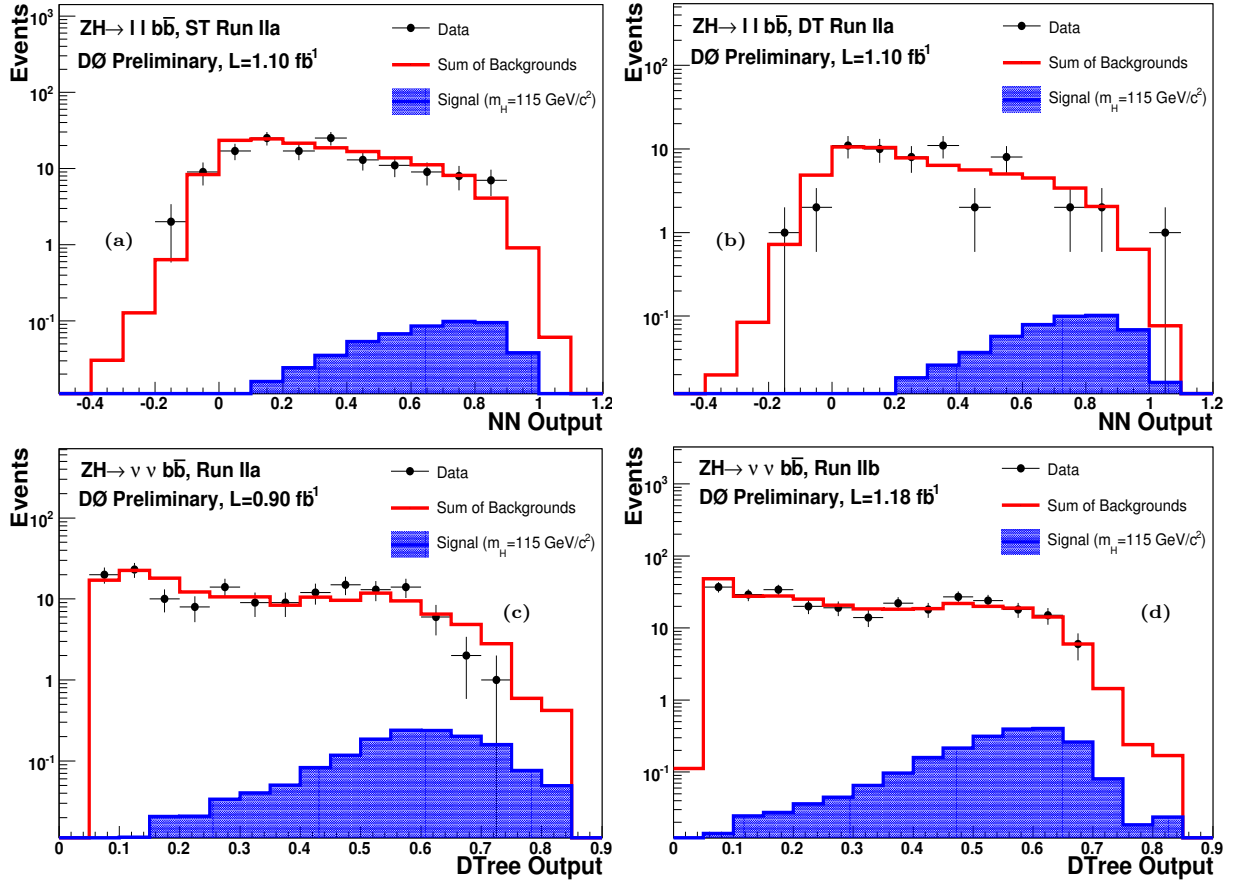


FIG. 2: Final variable distributions for  $p\bar{p} \rightarrow ZH \rightarrow \ell\ell/\nu\nu b\bar{b}$  Higgs search analyses. The figure contains distributions for: the NN discriminant for the Run IIa  $ZH \rightarrow \ell\ell b\bar{b}$  ST analyses (a), the NN discriminant for the Run IIa  $ZH \rightarrow \ell\ell b\bar{b}$  DT analyses (b), the DTree discriminant for the Run IIa  $ZH \rightarrow \nu\nu b\bar{b}$  analysis (c), and the DTree discriminant for the Run IIb  $ZH \rightarrow \nu\nu b\bar{b}$  analysis (d). For each figure, the total signal and background expectations and the observed data are shown.

theoretical calculation. Further details on the systematic uncertainties are given in Table II.

The systematic uncertainties for background rates are generally several times larger than the signal expectation itself and are an important factor in the calculation of limits. As such, each systematic uncertainty is folded into the signal and background expectations in the limit calculation via Gaussian distribution. These Gaussian values are sampled for each Poisson MC trial (pseudo-experiment). Several of the systematic uncertainties, for example the jet energy scale uncertainty, impact the shape of the final variable. These shape-dependencies were preserved in the description of systematic fluctuations for each Poisson trial. Correlations between systematic sources are carried through in the calculation. For example, the uncertainty on the integrated luminosity is held to be correlated between all signals and backgrounds and, thus, the same fluctuation in the luminosity is common to all channels for a single pseudo-experiment. All systematic uncertainties originating from a common source are held to be correlated, as detailed in Tables II and III.

To minimize the degrading effects of systematics on the search sensitivity, the individual background contributions are fitted to the data observation by maximizing a profile likelihood function for each hypothesis [24]. The profile likelihood is constructed via a joint Poisson probability over the number of bins in the calculation and is a function of the nuisance parameters in the system and their associated uncertainties, which are given an additional Gaussian constraint associated with their prior predictions. The maximization of the likelihood function is performed over the nuisance parameters. A fit is performed to both the background-only and signal-plus-background hypotheses separately for each Poisson MC trial.

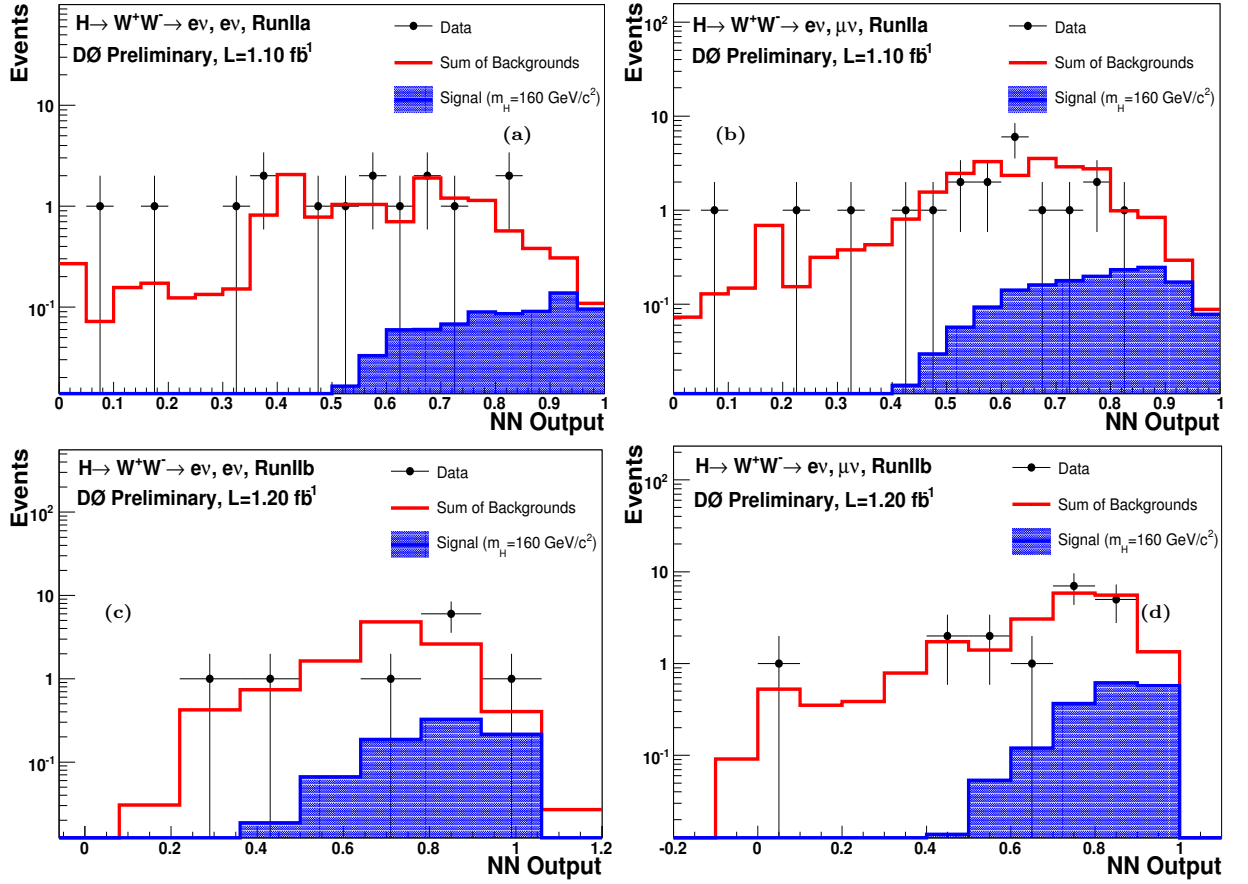


FIG. 3: Final variable distributions for selected Higgs search analyses. The figure contains distributions for: the NN discriminant for the Run IIa  $H \rightarrow W^+W^- \rightarrow e\nu, e\nu$  analysis (a), the NN discriminant for the Run IIa  $H \rightarrow W^+W^- \rightarrow e\nu, \mu\nu$  analysis (b), the NN discriminant for the Run IIb  $H \rightarrow W^+W^- \rightarrow e\nu, e\nu$  analysis (c), and the NN discriminant for the Run IIb  $H \rightarrow W^+W^- \rightarrow e\nu, \mu\nu$  analysis (d). For each figure, the total signal and background expectations and the observed data are shown.

### III. DERIVED UPPER LIMITS

We derive limits on SM Higgs boson production  $\sigma \times BR(H \rightarrow b\bar{b}/W^+W^-)$  via 25 individual analyses [4–10]. The limits are derived at a 95% C.L. To facilitate model transparency and to accommodate analyses with different degrees of sensitivity, we present our results in terms of the ratio of 95% C.L. upper cross section limits to the SM predicted cross section as a function of Higgs boson mass. The SM prediction for Higgs boson production would therefore be considered excluded at 95% C.L. when this limit ratio falls below unity. For the combined limit, the  $WH \rightarrow \ell\nu b\bar{b}$  and  $ZH \rightarrow \nu\bar{\nu} b\bar{b}$  signals are summed and their common background only enters the calculation once.

The individual analyses described above are grouped to evaluate combined limits over the range  $105 \leq m_H \leq 200 \text{ GeV}/c^2$ . The  $WH \rightarrow \ell\nu b\bar{b}$  and  $ZH \rightarrow \nu\bar{\nu} b\bar{b}$  analyses contribute to the region  $m_H \leq 145 \text{ GeV}/c^2$ , the  $ZH \rightarrow \ell\ell b\bar{b}$  analyses contribute for  $m_H \leq 155 \text{ GeV}/c^2$ , the Run IIa  $H \rightarrow W^+W^-$  and  $WH \rightarrow WW^+W^-$  analyses contribute for  $m_H \geq 120 \text{ GeV}/c^2$ , the Run IIb  $H \rightarrow W^+W^-$  analyses contribute for  $m_H \geq 115 \text{ GeV}/c^2$ , and the  $H \rightarrow \gamma\gamma$  analyses contribute for  $m_H \leq 150 \text{ GeV}/c^2$ .

Figure 5 shows the expected and observed 95% C.L. cross section limit ratio to the SM cross sections for all analyses combined over the probed mass region ( $105 \leq m_H \leq 200 \text{ GeV}/c^2$ ). The LLR distributions for the full combination are shown in Fig. 6. Included in these figures are the median LLR values for the signal-plus-background hypothesis ( $LLR_{s+b}$ ), background-only hypothesis ( $LLR_b$ ), and the observed data ( $LLR_{obs}$ ). The shaded bands represent the 1 and 2 standard deviation ( $\sigma$ ) departures for  $LLR_b$ . These distributions can be interpreted as follows:

- The separation between  $LLR_b$  and  $LLR_{s+b}$  provides a measure of the discriminating power of the search. This is the ability of the analysis to separate the  $s + b$  and  $b$ -only hypotheses.

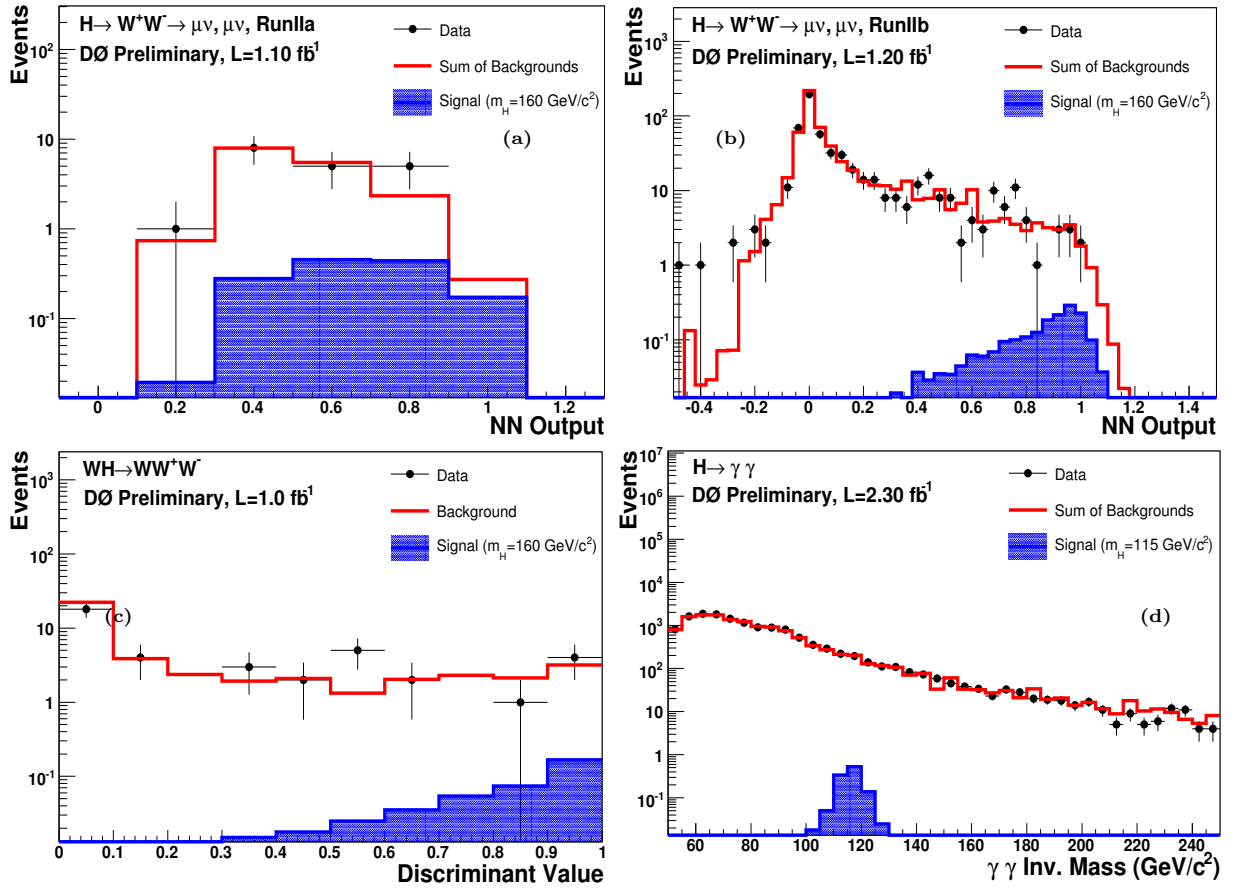


FIG. 4: Final variable distributions for selected Higgs search analyses. The figure contains distributions for: the NN discriminant for the Run IIa  $H \rightarrow W^+W^- \rightarrow \mu\nu, \mu\nu$  analysis (a), the NN discriminant for the Run IIb  $H \rightarrow W^+W^- \rightarrow \mu\nu, \mu\nu$  analysis (b), a one-dimensional projection of the two-dimensional likelihood for the Run IIa  $WH \rightarrow WW^+W^-$  analyses (c), and the diphoton invariant mass for the Run IIa and Run IIb  $H \rightarrow \gamma\gamma$  analyses combined (d). For each figure, the total signal and background expectations and the observed data are shown.

- The width of the  $LLR_b$  distribution (shown here as one and two standard deviation ( $\sigma$ ) bands) provides an estimate of how sensitive the analysis is to a signal-like background fluctuation in the data, taking account of the presence of systematic uncertainties. For example, when a  $1\sigma$  background fluctuation is large compared to the signal expectation, the analysis sensitivity is thereby limited.
- The value of  $LLR_{obs}$  relative to  $LLR_{s+b}$  and  $LLR_b$  indicates whether the data distribution appears to be more like signal-plus-background or background-only. As noted above, the significance of any departures of  $LLR_{obs}$  from  $LLR_b$  can be evaluated by the width of the  $LLR_b$  distribution.

#### IV. CONCLUSIONS

We have presented limits on standard model Higgs boson production derived from 25 Higgs search analyses. We have combined these analyses and form new limits more sensitive than each individual limit. The observed (expected) 95% C.L. limit ratios to the SM Higgs boson production cross sections are 6.4 (5.5) at  $m_H = 115 \text{ GeV}/c^2$  and 2.2 (2.4) at  $m_H = 160 \text{ GeV}/c^2$ .

TABLE II: List of leading correlated systematic uncertainties. The values for the systematic uncertainties are the same for the  $ZH \rightarrow \nu\bar{\nu}b\bar{b}$  and  $WH \rightarrow \ell\nu b\bar{b}$  channels. All uncertainties within a group are considered 100% correlated across channels. The correlated systematic uncertainty on the background cross section ( $\sigma$ ) is itself subdivided according to the different background processes in each analysis.

Source	$WH \rightarrow e\nu b\bar{b}$ DT(ST)	$WH \rightarrow \mu\nu b\bar{b}$ DT(ST)	$WH \rightarrow WW^+W^-$	$H \rightarrow W^+W^-$
Luminosity (%)	6.1	6.1	-	-
Normalization (%)	-	-	6.1	4-6
Jet Energy Scale (%)	3.0	3.0	0	3.0
Jet ID (%)	3.0	3.0	-	-
Electron ID/Trigger (%)	6.0	-	11	3-10
Muon ID/Trigger (%)	-	11.0	11	7.7-10
$b$ -Jet Tagging (%)	9.2(4.6)	9.2(4.6)	-	-
Background $\sigma$ (%)	6-20	6-20	6-18	6-18
Signal $\sigma$ (%)	0	0	0	10.0
QCD multijets (%)	14	14	30-50	15-40

Source	$ZH \rightarrow \nu\bar{\nu}b\bar{b}$	$ZH \rightarrow e^+e^-b\bar{b}$ DT(ST)	$ZH \rightarrow \mu^+\mu^-b\bar{b}$ DT(ST)	$H \rightarrow \gamma\gamma$
Luminosity (%)	6.1	6.1	-	6.1
Normalization (%)	-	-	6.1	-
Jet Energy Scale (%)	3.0	2.0	2.0	-
Jet ID (%)	2.0	5.0	5.0	-
Jet Triggers (%)	5.5	-	-	-
Electron ID/Trigger (%)	0	4.0	-	12-17
Muon ID/Trigger (%)	0	-	4.0	-
$b$ -Jet Tagging (%)	6.0	7.5(3.0)	7.5(3.0)	-
Background $\sigma$ (%)	6-16	10-30	10-30	5-26
Heavy-Flavor Scale (%)	50	-	-	-
QCD multijets (%)	-	41-50	50	20

TABLE III: The correlation matrix for the analysis channels. The correlations for the  $ZH \rightarrow \nu\bar{\nu}b\bar{b}$  and  $WH \rightarrow \ell\nu b\bar{b}$  channels are held to be the same. All uncertainties within a group are considered 100% correlated across channels. The correlated systematic uncertainty on the background cross section ( $\sigma$ ) is itself subdivided according to the different background processes in each analysis.

Source	$WH \rightarrow \ell\nu b\bar{b}$	$ZH \rightarrow \nu\bar{\nu}b\bar{b}$	$ZH \rightarrow \ell\ell b\bar{b}$	$H \rightarrow W^+W^-$	$WH \rightarrow WW^+W^-$	$H \rightarrow \gamma\gamma$
Luminosity	×	×	×			×
Normalization			×	×	×	
Jet Energy Scale	×	×	×	×		
Jet ID	×	×	×			
Electron ID/Trigger	×		×	×	×	×
Muon ID/Trigger	×		×	×	×	
$b$ -Jet Tagging	×	×	×			
Background $\sigma$	×	×	×	×	×	×
Signal $\sigma$				×		
QCD multijets (%)						

TABLE IV: Combined 95% C.L. limits on  $\sigma \times BR(H \rightarrow b\bar{b}/W^+W^-)$  for SM Higgs boson production. The limits are reported in units of the SM production cross section times branching fraction.

$m_H$ ( GeV/ $c^2$ )	105	115	125	135	140	150	160	170	180	190	200
Expected	4.4	5.5	6.9	6.4	5.5	3.9	2.4	2.9	3.6	5.8	8.7
Observed	4.1	6.4	11.6	10.8	8.6	3.2	2.2	2.6	3.9	4.2	6.5

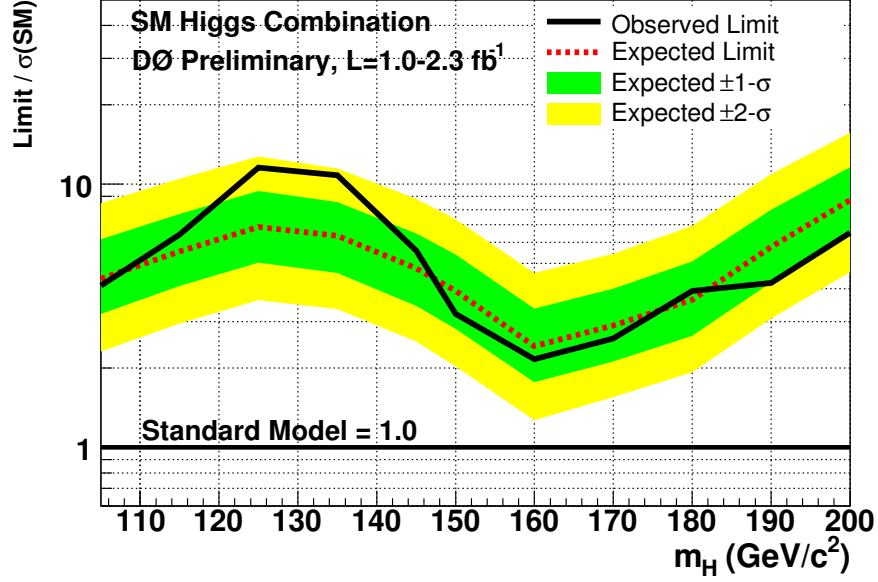


FIG. 5: Expected (median) and observed 95% C.L. cross section limit ratios for the combined  $WH/ZH/H, H \rightarrow b\bar{b}/W^+W^-/\gamma\gamma$  analyses over the  $105 \leq m_H \leq 200$   $\text{GeV}/c^2$  mass range.

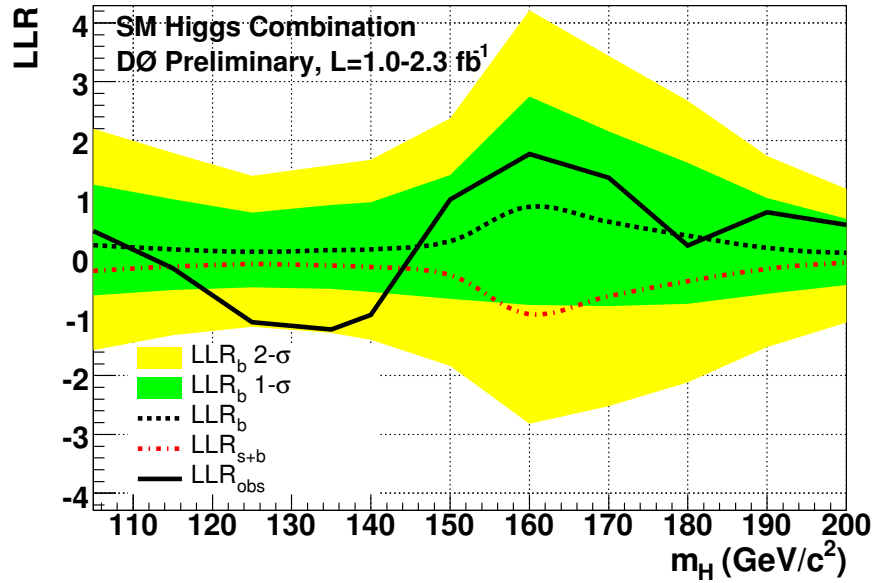


FIG. 6: Log-likelihood ratio distribution for the combined  $WH/ZH/H, H \rightarrow b\bar{b}/W^+W^-/\gamma\gamma$  analyses over the  $105 \leq m_H \leq 200$   $\text{GeV}/c^2$  mass range.

### Acknowledgments

We thank the staffs at Fermilab and collaborating institutions, and acknowledge support from the DOE and NSF (USA), CEA and CNRS/IN2P3 (France), FASI, Rosatom and RFBR (Russia), CNPq, FAPERJ, FAPESP and FUNDUNESP (Brazil), DAE and DST (India), Colciencias (Colombia), CONACyT (Mexico), KRF and KOSEF (Korea), CONICET and UBACyT (Argentina), FOM (The Netherlands), STFC (United Kingdom), MSMT and GACR (Czech Republic), CRC Program, CFI, NSERC and WestGrid Project (Canada), BMBF and DFG (Germany), SFI (Ireland), The Swedish Research Council (Sweden), CAS and CNSF (China), and the Alexander von Humboldt

Foundation.

- 
- [1] R. Barate *et al.* [LEP Working Group for Higgs boson searches], Phys. Lett. B **565**, 61 (2003), [arXiv:hep-ex/0306033].
  - [2] LEP Electroweak Working Group: <http://lepewwg.web.cern.ch/LEPEWWG/plots/winter2007/>.
  - [3] DØ Collaboration, V. Abazov *et al.*, Nucl. Instrum. Meth. A **565**, 463 (2006) [arXiv:hep-ph/0507191].
  - [4] DØ Collaboration, DØ Note 5472-CONF.
  - [5] DØ Collaboration, DØ Note 5586-CONF.
  - [6] DØ Collaboration, DØ Note 5482-CONF.
  - [7] DØ Collaboration, DØ Note 5485-CONF.
  - [8] DØ Collaboration, DØ Note 5537-CONF.
  - [9] DØ Collaboration, DØ Note 5624-CONF.
  - [10] DØ Collaboration, DØ Note 5601-CONF.
  - [11] T. Scanlon, FERMILAB-THESIS-2006-43.
  - [12] DØ Collaboration, DØ Note 5504-CONF.
  - [13] T. Sjöstrand, P. Edén, C. Friberg, L. Lönnblad, G. Miu, S. Mrenna and E. Norrbin, Computer Phys. Commun. **135** 238 (2001) [arXiv:hep-ph/0010017].
  - [14] J. Pumplin *et al.*, JHEP **0207**, 012 (2002).
  - [15] S. Catani *et al.*, JHEP **0307**, 028 (2003) [arXiv:hep-ph/0306211].
  - [16] K. A. Assamagan *et al.* [Higgs Working Group Collaboration], arXiv:hep-ph/0406152.
  - [17] A. Djouadi, J. Kalinowski and M. Spira, Comput. Phys. Commun. **108**, 56 (1998) [arXiv:hep-ph/9704448].
  - [18] M. L. Mangano *et al.*, JHEP **0307**, 001 (2003) [arXiv:hep-ph/0206293].
  - [19] A. Pukhov *et al.*, arXiv:hep-ph/9908288.
  - [20] <http://mcfm.fnal.gov/>.
  - [21] T. Junk, Nucl. Instrum. Meth. A **434**, 435 (1999); A. Read, CERN 2000-005 (30 May 2000).
  - [22] K. S. Cranmer, Comput. Phys. Commun. **136**, 198 (2001) [arXiv:hep-ph/0011057].
  - [23] A. Read, Nucl. Instrum. Meth. A **425**, 357 (1999).
  - [24] W. Fisher, FERMILAB-TM-2386-E.